STRUCTURAL DYNAMICS OBSERVATIONS IN SPACE LAUNCH SYSTEM GREEN RUN HOT FIRE TESTING

Richard K. Moore[*] **, John H. Wall**[†] **, Abran Alaniz***, **Stephen G. Ryan**[‡] **, Colter W. Russell**[§] **, Jeb S. Orr**[¶] **, Robert Towner**[‖] **and Jonathan Band**[**]

The Space Launch System (SLS) Core Stage (CS) Thrust Vector Control (TVC) system is comprised of eight mechanical feedback Shuttle heritage Type III TVC actuators and four RS-25 engines, each attached to a Shuttle heritage gimbal block/bearing. Two actuators are used to move each engine in two planes perpendicular to one another (i.e., pitch and yaw). The TVC system design leverages hardware from the Space Shuttle program as well as new hardware designed specifically for the Core Stage.

The Green Run Hot Fire (GRHF) of the SLS Core Stage provided a flight-like ground test environment for verification of integrated vehicle TVC performance. A TVC model coupled to a vehicle structural dynamic model has been developed previously and incrementally validated in subsystem tests and simulations. Still, some aspects of TVC performance in GRHF were not anticipated. The ensuing investigation demonstrated the need for well-instrumented test environments, various levels of modeling fidelity, test-representative structural models, and caution in reuse of legacy components.

This paper is the sixth installment in a seven-paper series surveying the design, engineering, test validation, and flight performance of the Core Stage Thrust Vector Control system. It introduces the salient structural dynamic phenomena uncovered in ambient and hot fire testing. During the Green Run test campaign, a comparison of ambient and hot fire step responses showed a significant change in apparent damping due to the presence of friction, challenging long standing assumptions that friction could be neglected. Additionally, the characteristic response of the engine and thrust structure during GRHF proved to be more complex than anticipated, as evidenced by the available actuator, thrust structure, and engine measurements. While the string-potentiometer based test instrumentation was intended to allow for reconstruction of the engine angles along the two control axes, the geometric placement, location uncertainty, and responses in overlapping frequency spectra revealed additional phenomena requiring further analysis and post-processing. The observations from both modal and frequency response testing during the Green Run ambient and hot fire configurations led to Engine and Core Stage FEM (finite element model) updates. When evidence of unexpected engine motion was found in engine section accelerometer data, the authors pursued additional structural analysis leading to FEM updates associated with the TVC gimbal and thrust structure. Through collaboration between structures, TVC, and flight control disciplines, the test-informed models and root-cause analysis led to confident flight rationale for the first flight of the SLS launch vehicle.

[*]Flight Systems Principal Staff, Mclaurin Aerospace (Jacobs ESSCA)

[†]SLS Flight Controls Lead, Mclaurin Aerospace (Jacobs ESSCA), Huntsville, AL

[‡]SLS Chief Engineer's Office (MTS CPSS), Huntsville, AL

[§]Flight Systems Technical Staff, Mclaurin Aerospace (Jacobs ESSCA), Knoxville, TN

[¶]Space Launch System Flight Dynamics and Control Technical Specialist (Mclaurin Aerospace / ESSCA), Knoxville, TN

[‖]Technical Fellow for Loads and Dynamics, Jacobs Technology (Jacobs ESSCA)

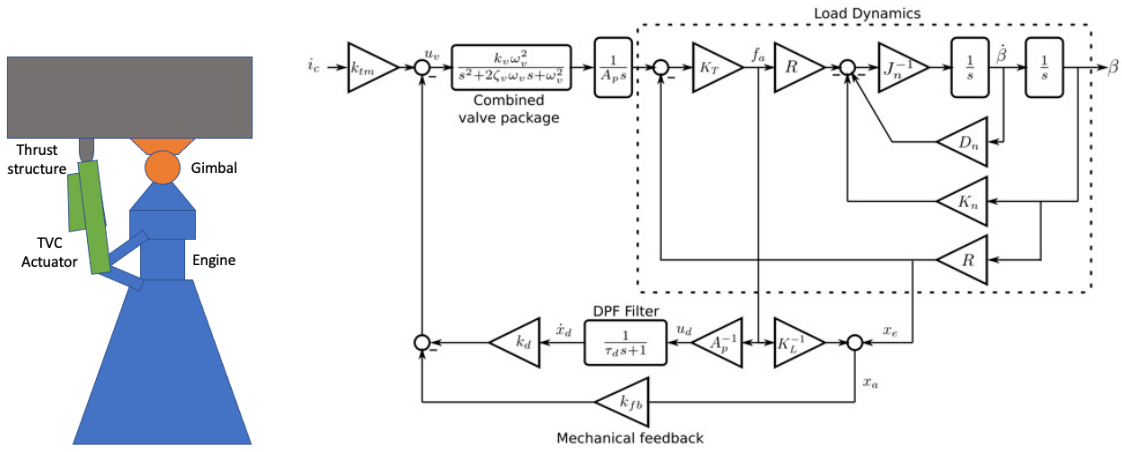[**]Structural Dynamics Engineer, NASA Marshall Space Flight Cetner

Figure 1. a. Physical TVC diagram. b. Simplex TVC model block diagram.

1 INTRODUCTION

Each of the four RS-25E engines on the SLS Core Stage is mounted to a spherical gimbal and actuated in pitch and yaw by separate mechanical feedback hydraulic actuators. To support flight control analyses, each thrust vector control degree of freedom can be expressed by the control diagram in Figure 1 and as a linear state space representation.[5] The resulting set of coupled differential equations describe the behavior of the engine angle, β, and the actuator piston displacement, x_a (which provides the feedback for control), in response to a command current. Since the engines and actuators are mounted to a common thrust structure, an avenue exists for structural coupling among actuators. Prior work has extended this linear state space formulation (referred to as the "Simplex" model) to eight actuators coupled through a finite-element modal model of the vehicle and engine structures. The resulting expanded formulation has been mechanized in the MASV (Multiple Actuator Stage Vectoring) tool to study the TVC system coupling with the structural dynamics at Marshall Space Flight Center during SLS development.[5]

Finite element analysis of the coupled engine and vehicle structures predicts a dense set of modes within the TVC bandwidth, as shown by the number of prominent peaks in the Figures 2a and 2b, where the force-to-actuator displacement response has been generated using a simple spring representation for the actuator. Because of this, structural dynamics can couple with the TVC response.[1] While no individual structural mode dominates the TVC response, the modally-integrated load stiffness places a pair of complex zeroes in the system which are observable in the piston position telemetry as the load resonance notch in the frequency response. For this reason the notch is at nearly the same frequency for MASV bode plots in Figure 2 with either static or dynamic vehicle modes. The structure-coupled TVC system model predicts some modest differences in response for the eight different actuator locations, but the MASV bode plots in Figures 2c and 2d for the engine 1 pitch actuator are largely representative of the expected piston and associated engine angle responses of the SLS core stage TVC in the ambient and hot fire test conditions.

The actuator piston is the only measurement of engine motion available in flight telemetry, so verifying the modeled relationship between the piston position and engine angle was an important
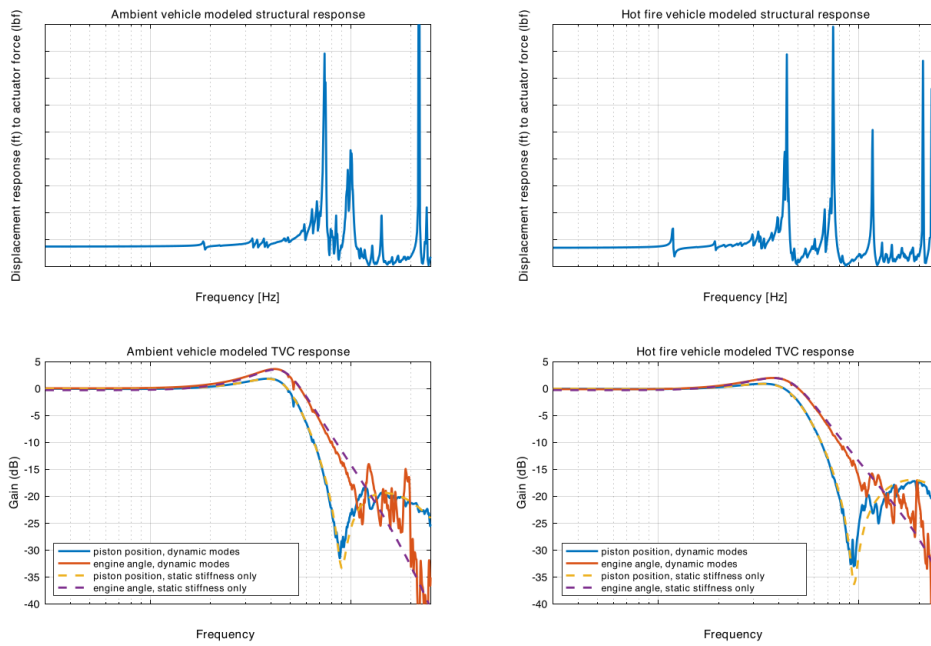
2

Figure 2. a. Modeled structural response of the ambient vehicle. b. Modeled structural response of the hot fire vehicle. c. Modeled (MASV) ambient vehicle TVC response. d. Modeled (MASV) hot fire vehicle TVC response.

goal in the Green Run test campaign for SLS. Load-dependent stiffnesses in the actuator and gimbal were found to introduce additional dynamics during ambient testing which complicated structural model verification. However, hot fire testing demonstrated that the loaded actuators and gimbal operate in linear portions of their stiffness curves.

The hot fire frequency and step response testing also showed that the effects of thrust-loaded gimbal bearing friction significantly affected the responses. The development and fitting of an appropriate friction model for the thrust-loaded SLS core stage has been provided by Russell.[6] The presence of friction drove a need for the modeling of gimbal translational and torsional stiffnesses, which had been represented as rigid body elements in earlier versions of the finite element models.

2 TEST CAMPAIGN

A series of test activities were used to validate the models and parameter values for the actuator, vehicle & engine structures, and coupled interaction between actuators & structure under successively more mission-representative conditions. For investigation of isolated actuator behavior, a lab was set up at MSFC using a Type III actuator with flight-like gimbal and actuator attach points driving a mass simulator of an RS25 engine. Wall provides a more comprehensive description of this actuator testing lab.[7] Modal testing of the assembled Core Stage and attached engines for structural model verification took place at Stennis Space Center. Structure-coupled TVC actuator response testing was then iteratively characterized on the assembled vehicle at ambient conditions, during Green Run Hot Fire, and during the Artemis I test flight mission.[9]
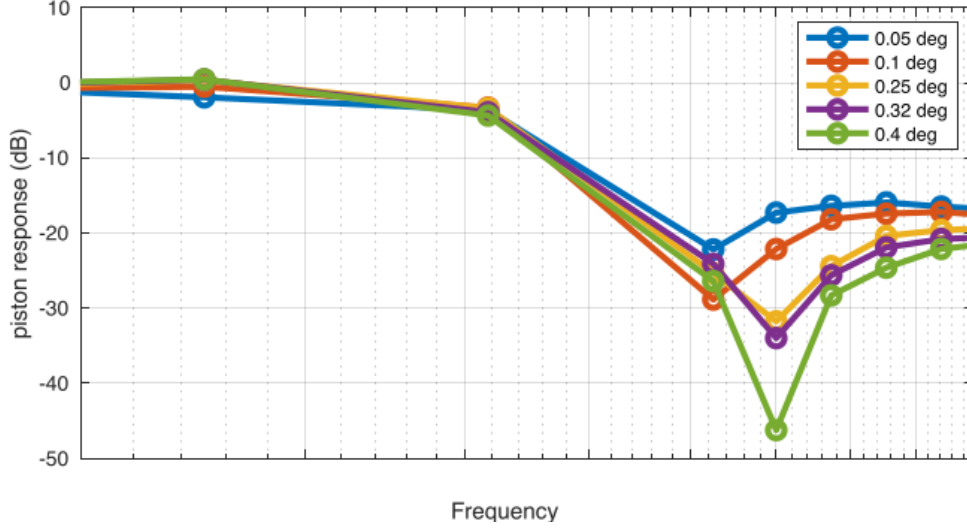
Figure 3. Measured piston response from the actuator lab showing amplitude-dependent load frequency notch.

2.1 Actuator Lab Testing

The primary focus of actuator lab testing was to characterize the non-structural portions of the thrust vector control system. For this reason, much of that testing is outside the scope of this paper. However, some performance-impacting structural phenomena were observed in this environment. Figure 3 shows command-amplitude-dependent frequency response in a region where linear operation was expected.

This behavior is not consistent with smaller previously identified nonlinearities in the servovalve actuator. To support further investigation, the MIMO Simplex state space model can be reduced to a SISO system to obtain a transfer function from actuator commands to piston position. While the full solution is cumbersome to present, it can be readily computed with a computer algebra system. The resulting transfer function has a complex zero pair at the load resonance notch:

$$\frac{-\left(D_n \pm \sqrt{D_n^2 - 4J_n K_L R^2 - 4J_n K_n}\right)}{2J_n} \tag{1}$$

Ignoring the duct stiffness K_n, which was not present in these actuator lab measurements (associated torsion rods were disengaged), and the negligible viscous damping term D_n, the resulting characteristic frequency is:

$$\omega_L = \sqrt{\frac{K_L R^2}{J_n}} \tag{2}$$

Values for the moment arm R and inertia J_n are readily available from the test stand mechanical design. Changes in the observed characteristic frequency are therefore the sole result of a change in the load stiffness, K_L. The system stiffness will be further divided into two constituent stiffnesses
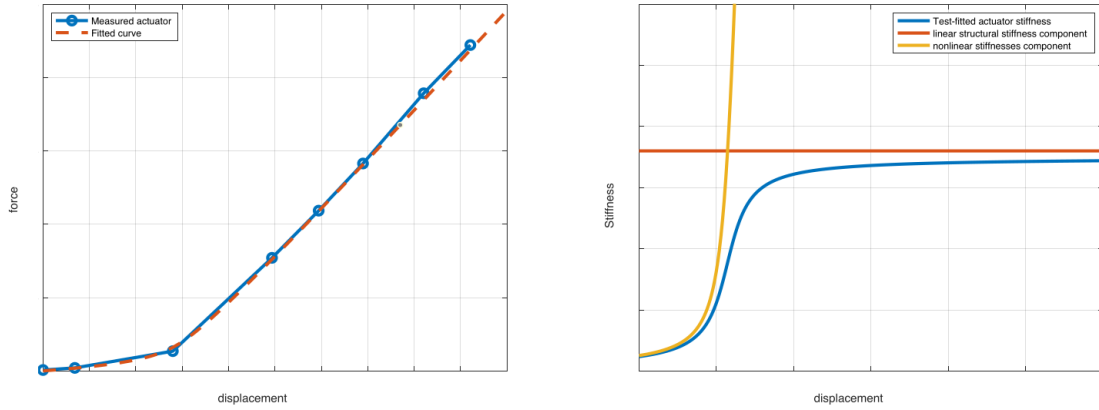
Figure 4. a. Force vs displacement curve for Type III actuator (measured by the vendor) exhibiting nonlinear stiffness. b. Constituent and overall stiffness curves for the actuator.

in series representing the engine mass simulator itself, K_{ES}, and the portion of the actuator stiffness which falls outside of the loop closure, K_{act}:

$$K_L = \frac{1}{\frac{1}{K_{ES}} + \frac{1}{K_{act}}}$$ (3)

Prior testing from the actuator supplier demonstrated reduced outside-the-loop stiffness for loads under 2000 lbf.[3] The overall length change of the powered actuator was measured as a function of force applied to the actuator ends. Since mechanical feedback zeroes the actuator piston position error, the represented stiffness is for actuator components outside of the feedback loop. While individual stiffness testing of the actuator components is not available, analysis from the vendor indicates that the the stiffness is largely linear and due to structure when loaded with greater than several thousand pounds of force. For lower loads the stiffness exhibits significant nonlinearities which are expected to be due to a number of factors, including spherical bearing loading and oil stiffness while the servovalve is in dead band. Measured and modeled functions related to dynamic actuator stiffness are provided in Figure 4. A curve was fit to the vendor test data to support TVC performance modeling.

The fitted actuator stiffness function was incorporated with the appropriate stiffness blocks of a Simulink implementation of the Simplex model. The numerical results from the resulting set of nonlinear differential equations are presented in Figures 5, 7, and 8.

Alternatively, the amplitude-dependent shift in apparent load stiffness due to the actuator nonlinearity can be estimated by taking a weighted average of stiffness over the appropriate region of the stiffness curve. This region spans from the nominal actuator load force to the command-dependent peak force. Peak force was not logged directly during actuator lab frequency response testing, but can be calculated from available terms: the engine mass simulator inertia J_n, the moment arm R, and the angular acceleration α obtained from the second derivative of the sine commands, with amplitude a and radian frequency b. The calculated maximum force can then be used to estimate the peak actuator displacement x_{max} using the curve in Figure 4:
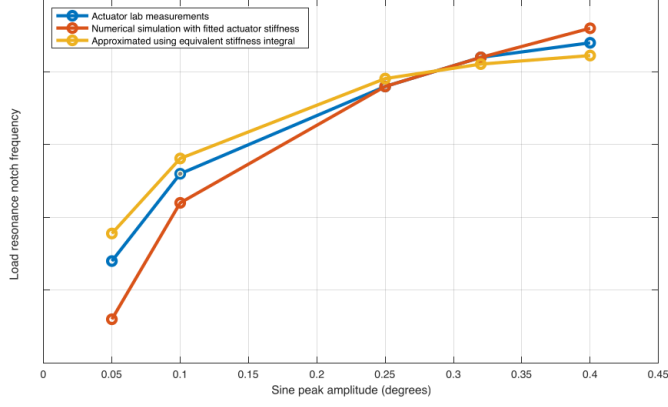
Figure 5. Measured and modeled relationship between command amplitude and notch frequency.

$$\alpha = \frac{d^2}{dt^2}\left(a\sin bt\right) = -ab^2\sin bt \tag{4}$$

$$f_{max}\left(a,b\right) = \frac{J_n\alpha_{max}\left(a,b\right)}{R} \tag{5}$$

For peak actuator displacement x_{max} the weighted average of the actuator stiffness may be estimated with the integral:

$$\int_0^{x_{max}} f\left(x\right)dx = \int_0^{x_{max}} K_{act}xdx \tag{6}$$

$$\bar{K}_{act} = \frac{2}{x_{max}^2}\int_0^{x_{max}} f\left(x\right)dx \tag{7}$$

Both the results from the Simplex model (augmented to include the nonlinear actuator stiffness) and the equivalent stiffness integral above largely agree with the amplitude-dependent load resonance observed in the actuator lab, as is shown in Figure 5.

2.2 Vehicle and Engine Modal Testing

Modal testing was conducted on the assembled Core Stage to verify the structural load characteristics.[2] A mechanical lock was placed on the unpowered actuators to exclude dynamics from the closed-loop servovalves. For this case the state space representation simplifies to a single second order ordinary differential equation:

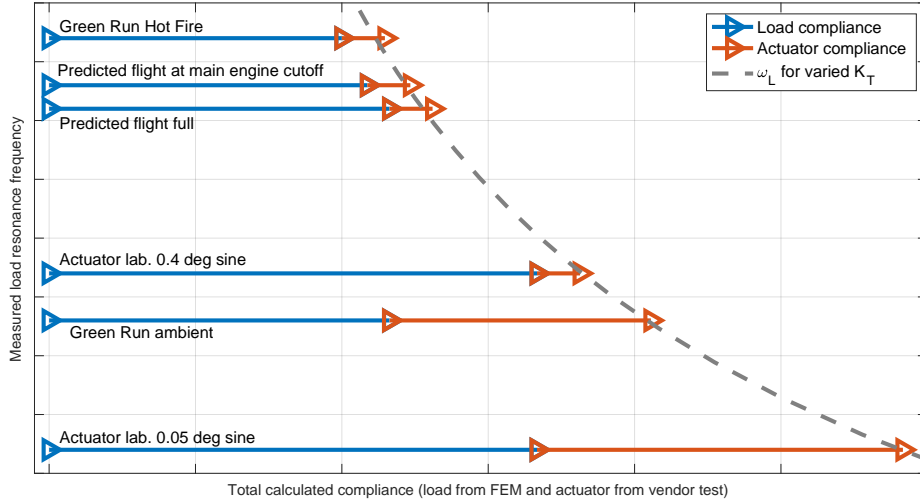$$\ddot{\beta} + \frac{D_n}{J_n}\dot{\beta} + \left(\frac{K_n + K_T R^2}{J_n}\right)\beta = 0 \tag{8}$$

6

Figure 6. Comparison of calculated compliances, test-measured load resonances, and the ideal ω_L curve for varied K_T

Here K_T is the total stiffness, representing the reciprocal sum of the two series stiffnesses for the structural load, K_L, and the actuator, K_{act}:

$$K_T = \frac{1}{\frac{1}{K_{act}} + \frac{1}{K_L}} \tag{9}$$

Some algebraic manipulation reveals that the characteristic frequency of this system can be expressed as:

$$\omega_0 = \sqrt{\frac{K_n + K_T R^2}{J_n}} \tag{10}$$

The duct stiffness term K_n which was excluded from the earlier actuator lab data analysis is reintroduced here. Response accelerometers were installed on the engines. The engines were then excited with a modal hammer. Modal correlation revealed that an engine pendulum motion was noted at 6.75 Hz. This was initially at odds with structural modeling, which predicted the engine pendulum mode between 7.5 and 8 Hz. Incorporating the low stiffness exhibited by the unloaded actuator which was noted in actuator testing, however, lowers the predicted total resonance to within the range of the observed frequencies of the engine pendulum-type modes.

With stiffnesses from FEM modal integrals of the different vehicle configurations and effective actuator stiffnesses calculated from force curve integrals centered about the nominal load, the different load resonance frequencies observed under the different test conditions can be modeled. FEM-calculated vehicle stiffnesses, force-integrated effective stiffnesses, and test-measured total resonance frequencies are shown in figure 6 for the different TVC test and operation conditions.
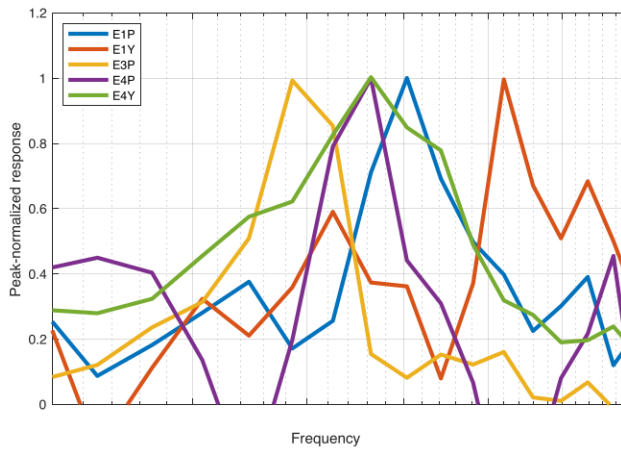
7

Figure 7. Piston spectra measured during quiescent periods of Core Stage modal testing

Additionally, piston position data was collected from the unlocked and powered but uncommanded actuators during a portion of the vehicle modal testing. The combination of the actuator falling inside servo/feedback deadbands and the presence of sufficient ambient excitations of the structure resulted in some engine motion observable in the piston telemetry logs. While not all actuators received sufficient ambient excitation to allow pendulum mode observation with the actuators unlocked, normalized responses for 5 of the 8 actuators are given in Figure 7. These show peaks at lower-than-flight-like frequencies in the 5.9-8.2 Hz range. Data was not available for the ambient excitations that drove these responses, but the response plots are included to demonstrate that the system measurements are confounded by the highly amplitude-dependent stiffness of the unloaded TVC actuators.

2.3 Ambient Thrust Vector Control Response Testing

The thrust vector control system was exercised with frequency response sine and step commands on the assembled Core Stage at ambient conditions (engines off, non-cryo, tanks empty, mounted to the test stand). Since the engine angle is not observed directly by the actuator piston, string potentiometers were installed as test ground truth instrumentation. Four such devices were installed per engine in the Core Stage engine section to monitor engine movement. Conversion from string length sets to engine angles was achieved using affine transforms fitted to commanded static engine angles after dynamic responses had settled out. Aligning with modal test and actuator lab measurements, the load resonance observed in actuator piston telemetry was lower than expected for flight conditions, but still consistent with the stiffness of Type III actuators without thrust loading.[7] Figure 8 shows the measured piston and engine responses along with modeled performance from Simplex with test-fitted actuator stiffness.

The step response of the Core TVC was investigated on the ambient vehicle as well. Figure 9 shows the step responses for the piston position and engine angle both measured during the Green Run ambient test and as modeled by Simplex with the nonlinear actuator stiffness. Friction is negligible in this vehicle configuration, resulting in the underdamped response. The observed overshoot was greater than initially expected, but represented in the model after the nonlinear actuator stiffness is incorporated.
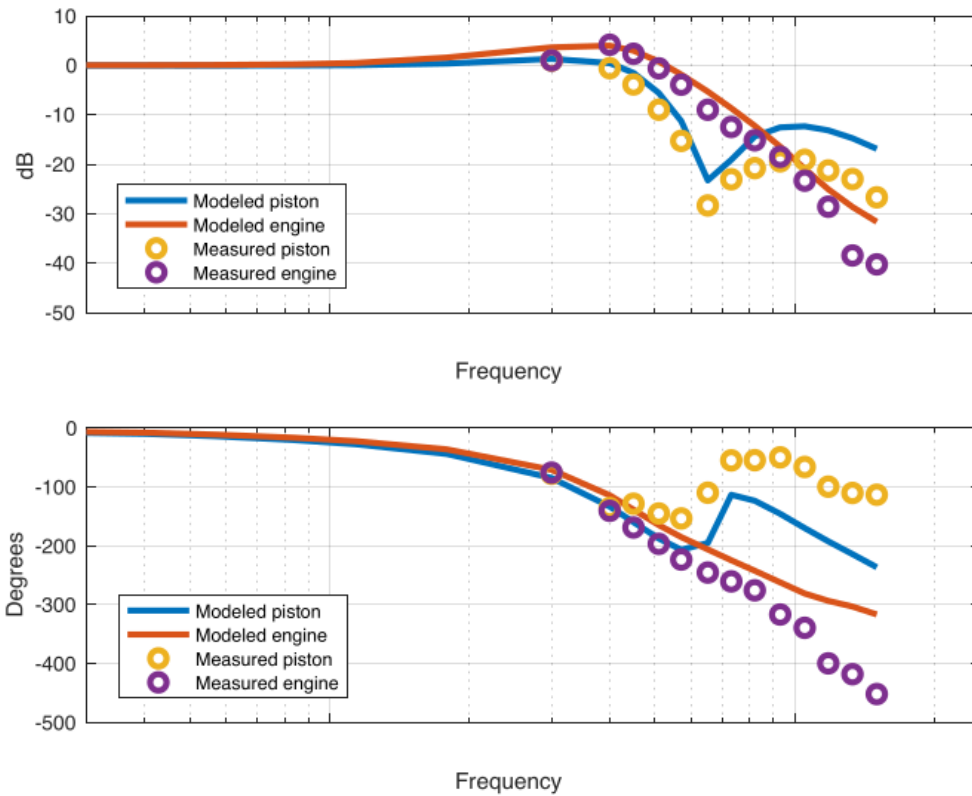
Figure 8. Measured and modeled (Simplex with nonlinear actuator stiffness) Green Run ambient test piston and engine responses.
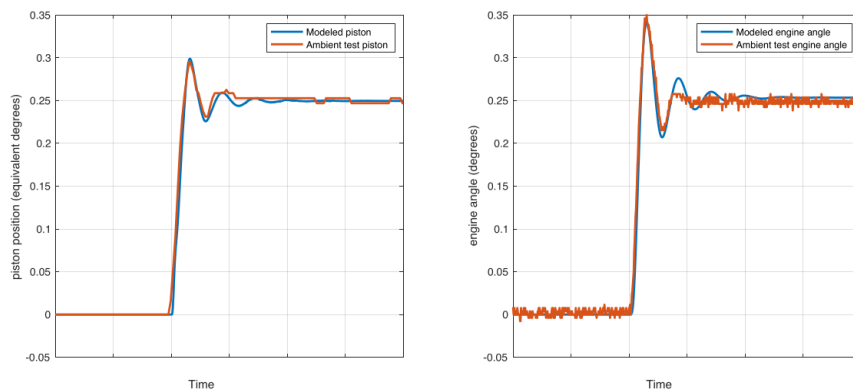

Figure 9. Green Run ambient measured and modeled (Simplex with nonlinear actuator stiffness) ambient step response.
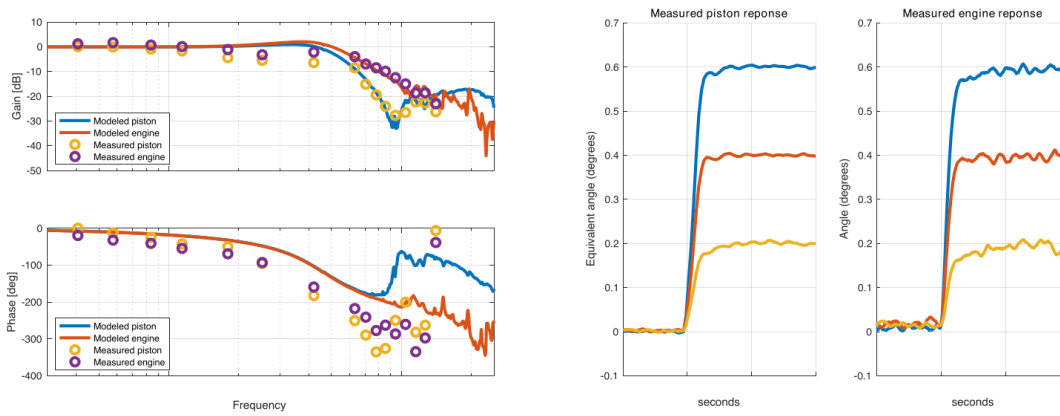
9

Figure 10. a. Green Run hot fire measured and modeled (MASV) piston and engine angle frequency responses. b. Green Run hot fire measured step responses.

While a practical means to achieve continuous nominal flight-like actuator loading during ambient vehicle testing has not been identified, sine sequences at multiple amplitudes can define a load resonance curve that approaches the flight-like stiffness asymptote. This method was developed after completion of the Artemis I vehicle testing, but has been demonstrated in the Actuator Lab, as shown in Figures 3 and 5.

2.4 Green Run Hot Fire Thrust Vector Control Response Testing

Green Run Hot Fire provided the only pre-flight opportunity to characterize the full thrust vector control system with engine thrust loading and a flight-like vehicle stiffness (at cryogenic temperatures with filled and re-pressurized tanks). The load frequency during Green Run Hot Fire was significantly different than during the ambient condition. Following Green Run testing, an updated FEM model of the gimbal structure was provided and evaluated in MASV. This update, along with the fact that the higher loads and higher amplitude command tests during Green Run eliminates the actuator stiffness nonlinearity, resulted in a very close match between model and test in the region of the notch frequency.

Some relatively small variations in modally integrated load stiffness for the different actuator locations were predicted by the finite element model. Per-actuator load stiffness was estimated in from the GRHF piston data with Simplex model curve fitting. The predicted and measured load stiffnesses are compared in Figure 11.

In addition to the shift in load resonance, the step responses show much more damping during hot fire testing than ambient testing. This damping has been attributed to gimbal friction. A comprehensive friction model for this behavior has been provided elsewhere by Russell.[6] Friction modeling efforts also revealed the opportunity to excite torsional displacement in the gimbal (particularly about the pitch and yaw axes) which further shapes the TVC response spectra. The prior finite element model of the Core stage had represented the gimbals as simple rigid body elements with no compliance. To properly model the forces and torques introduced by gimbal friction on a compliant gimbal, the SLS structural analysis team investigated the gimbal design and updated the Core Stage finite element models accordingly.[4] The TAOS (Two Axis Operational Simulation) models phenomena beyond the scope of the linear Simplex model including gimbal motion degrees of free-
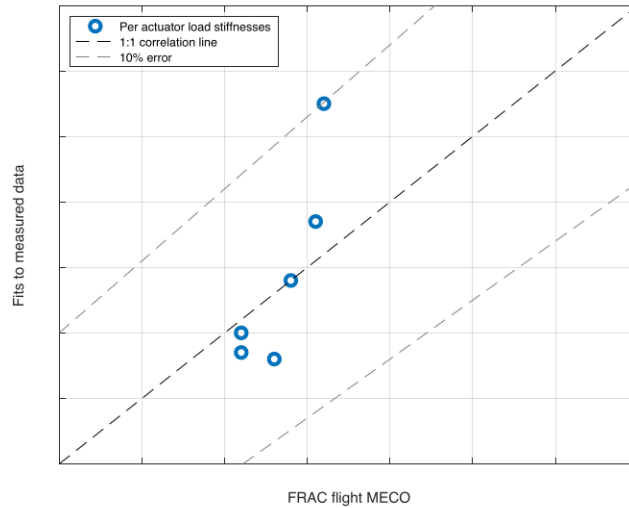
10

Figure 11.   Comparison of load stiffnesses measured (apparent load stiffness from Green Run hot fire piston notch) and predicted (FEM modal integral)

dom, gimbal friction, and nonlinear actuator stiffness. Figure 12 presents TAOS results showing that friction effects eliminate the load resonance notch unless gimbal compliances are represented in the model.

3   CONCLUSION

While a significant body of prior test and flight data existed for the RS-25E engines and Type III actuators prior to the SLS Green Run test campaign, the incremental SLS test campaign revealed previously unmodeled structural phenomena important to modeling SLS TVC behavior at ambient conditions. The load-dependent stiffnesses of the actuators and gimbal along with the ambient vehicle significantly lower the observed load resonance. A multiple-sine method was identified to determine structure-coupled loaded-actuator TVC performance from vehicle measurements at am-
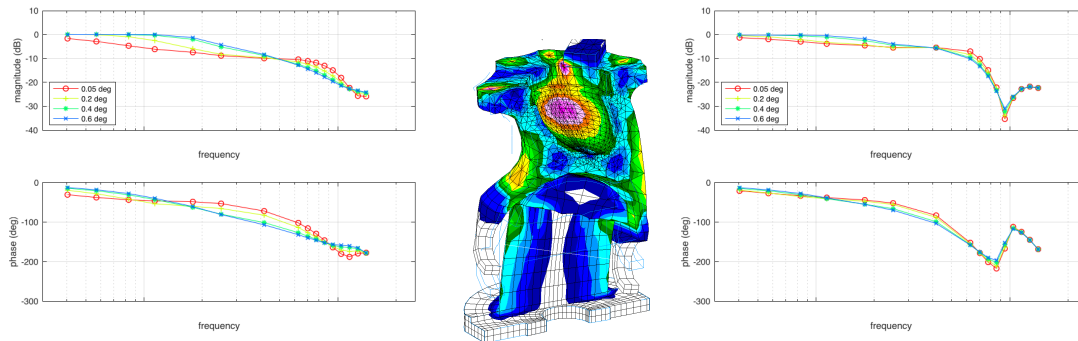

Figure 12. a. TAOS (Two Axis Operational Simulation) Modeled frequency response with friction prior to gimbal modeling in FEM. b. Illustration of torsional displacement of the friction locked gimbal. c. TAOS Modeled frequency response with friction and coupled gimbal stiffness.

bient conditions. This will inform operational checks of TVC on future SLS vehicles which are not expected to have hot fire tests. Friction was found to impact TVC performance significantly, providing not only damping but also frequency domain shaping from friction-coupled gimbal torsion loading during vectoring. The finite element models were updated to incorporate friction-relevant gimbal compliances not previously expected to influence TVC performance.

Overall, a significant need was demonstrated for a variety of developmental test environments and conditions to provide comprehensive scrutiny of the performance models and parameters used to support flight control analyses. Inevitably, some unanticipated behaviors were found at each stage of testing and needs emerged for analysis beyond the scope of the planned verification activities.

ACKNOWLEDGMENTS

REFERENCES

[1] Orr, J., Wall, J., and Barrows, T., "Simulation-Based Analysis and Prediction of Thrust Vector Servoelastic Coupling," AAS 20-091, American Astronautical Society Guidance, Navigation, and Control Conference, February 2020. 1

[2] Sontag, B. ,"Space Launch System (SLS) RS-25 Engine Pendulum Modal Test Report", SLS-DEV-20-024, 2020, NASA Marshall Space Flight Center, 2020. 2.2

[3] Beyer, W., "Type III Orbiter Actuator Static Stiffness",MCM-SLS-B189, Coordination Memo, 2014. 2.1

[4] Towner, R., "RS-25 Engine Gimbal Bearing Model Updates for Free-Hanging and Thrust-Loaded Conditions," Marshall Space Flight Center, 2022. 2.4

[5] Orr, J. , et al, "Advanced Modeling of Control-Structure Interaction in Thrust Vector Control Systems," American Astronautical Society, February 2023. 1

[6] Russell, C., et al, "Gimbal Bearing Friction in the Core Stage TVC System," American Astronomical Society, February 2023. 1, 2.4

[7] Wall, J., et al, "Design, Instrumentation, and Data Analysis for the SLS Core Stage Green Run Test Series," American Astronomical Society, February 2023. 2, 2.3

[8] Young, Warren C., Budynas, Richard G., Roark's Formulas for Stress and Strain, 2002.

[9] Wall, J., et al,"Flight Performance and Stability of Space Launch System Core Stage Thrust Vector Control," American Astronautical Society, February 2023. 2

[10] Stuart, B., et al., "Core Stage TVC Systems Engineering Challenges in Reusing Heritage Hardware," AAS 23-154, American Astronautical Society Guidance, Navigation, and Control Conference, February 2023.

[11] Stuart,B.,etal.,"OverviewoftheSLSCoreStageThrustVectorControlSystemDesign,"AAS23-152, American Astronautical Society Guidance, Navigation, and Control Conference, February 2023.